Non-Fermi-liquid behavior at the antiferromagnetic quantum critical point in the heavy-fermion system $Ce(Cu_{1-x}Co_x)_2Ge_2$

Rajesh Tripathi,[1] Debarchan Das,[1,2] C. Geibel,[2] S. K. Dhar,[3] and Z. Hossain[1,*]
[1]*Department of Physics, Indian Institute of Technology, Kanpur 208016, India*
[2]*Max Planck Institute for Chemical Physics of Solids, 01187 Dresden, Germany*
[3]*DCMP and MS, Tata Institute of Fundamental Research, Mumbai 400005, India*

(Received 6 March 2018; revised manuscript received 14 August 2018; published 24 October 2018)

Polycrystalline samples of $Ce(Cu_{1-x}Co_x)_2Ge_2$ were investigated by means of electrical resistivity $\rho(T)$, magnetic susceptibility $\chi(T)$, specific heat $C_p(T)$, and thermoelectric power $S(T)$ measurements. The long-range antiferromagnetic order, which set in at $T_N = 4.1$ K in $CeCu_2Ge_2$, is suppressed by non-isoelectronic cobalt doping at a critical value of the concentration $x_c = 0.6$, accompanied by non-Fermi-liquid behavior inferred from the power-law dependence of heat capacity and susceptibility, i.e., $C(T)/T$ and $\chi(T) \propto T^{-1+\lambda}$, down to 0.4 K, along with a clear deviation from T^2 behavior of the electrical resistivity. However, we have not seen any superconducting phase in the quantum critical regime down to 0.4 K.

DOI: 10.1103/PhysRevB.98.165136

I. INTRODUCTION

In some compounds of Ce and Yb, a second-order quantum phase transition (QPT) at $T \to 0$ separates the ordered and paramagnetic states and leads to interesting properties such as non-Fermi-liquid, heavy-fermion (HF) behavior and/or unconventional superconductivity. For example, the HF metal $CeCu_2Si_2$ and its sister analog $CeCu_2Ge_2$ both show superconductivity around their antiferromagnetic (AFM) quantum critical point (QCP) under pressure [1–3]. At ambient pressure, $CeCu_2Ge_2$ is an antiferromagnetically ordered heavy-fermion system (HFS) with Néel temperature $T_N = 4.1$ K and a characteristic Kondo lattice temperature $T^* = 6$ K [4], with similar energy scales of Kondo and RKKY interaction. With increasing pressure the hybridization between $4f$ and conduction electrons due to the Kondo effect increases, which suppresses antiferromagnetism and eventually superconductivity emerges. The superconductivity around AFM QCP is believed to be mediated by magnetic fluctuations, as inferred from neutron scattering experiments [5]. Superconductivity has also been observed in Ge-substituted $CeCu_2(Si_{1-x}Ge_x)_2$ [6] and Ni-substituted $Ce(Cu_{1-x}Ni_x)_2Si_2$ [7] around the AFM QCP. The quantum critical phenomenon and the associated non-Fermi-liquid (NFL) behavior in such cases arises due to the fluctuations of the AFM order parameter with diverging intensity at the QCP, as described in the spin fluctuation theories of Hertz, Millis, and Moriya (HMM) [8]. Although numerous investigations on $CeCu_2Ge_2$ have been carried out using high pressure, low temperature, and magnetic field, the effect of disorder on the physical properties close to the magnetic-nonmagnetic boundary has not been addressed.

The competition between the Ruderman-Kittel-Kasuya-Yosida (RKKY) and Kondo interactions in HFS offers the opportunity to tune these systems towards the magnetic-nonmagnetic boundary by alloying or hydrostatic pressure. It has been observed that the NFL behavior of some chemically substituted f-electron systems is better described within the context of Castro Neto theory based on Griffiths singularities [9–14]. At the QCP, NFL behavior in such systems is phenomenologically found to be described with $C(T)/T$ and $\chi(T) \propto T^{-1+\lambda}$, where λ is slightly smaller than 1.0 and a power law in the resistivity $\rho(T) = \rho_0 + AT^\alpha$ with either $\alpha \approx 1$ or 1.5 for 2D and 3D quantum fluctuations, respectively [13–16]. So far, many HFSs belonging to this category (alloying) have been investigated successfully with vanishing AFM phase transitions near the QCP, e.g., $CeCu_{6-x}Ag_x$ [17], $YbCu_{5-x}Al_x$ [18], and $Ti_{1-x}Sc_xAu$ [19]. In $Ce(Cu_{1-x}Ni_x)_2Ge_2$, the x-T phase diagram shows a transition from a local moment type of AFM ordering for $x < 0.2$ to a heavy-fermion band magnetism between $0.2 \leqslant x \leqslant 0.75$, and finally to a Fermi liquid close to $x = 1$ [20,21]. Compared to Cu($3d^{10}$), Ni ($3d^9$) has one less electron whereas Co($3d^8$) has two less electrons. Thus, it is expected that Co doping introduces more electronic disorder in the Cu-Ge layer. A preliminary report on $Ce(Cu_{1-x}Co_x)_2Ge_2$ [22] based only on resistivity and specific heat measurements exists in the literature indicating a possible critical concentration of $x =$ 0.5–0.6 for suppression of magnetic order. Here, $CeCo_2Ge_2$ is an intermediate-valence/heavy-fermion compound with relatively high Kondo temperature (T_K) [23]. In the present work, we have carried out a comprehensive study of the low-temperature properties of $Ce(Cu_{1-x}Co_x)_2Ge_2$ by means of electrical resistivity $\rho(T)$, magnetic susceptibility $\chi(T)$, heat capacity $C_p(T)$, and thermoelectric power $S(T)$ measurements. Besides making more compositions with various values of x than in Ref. [22], we report on the magnetic susceptibility and the thermopower data in this system. Our results show that the AFM ground state of $CeCu_2Ge_2$ can be continuously suppressed by Co doping and around the critical concentration $x_c \sim 0.6$ there are indications of a breakdown of FL behavior; in particular, the heat capacity divided by

*zakir@iitk.ac.in

temperature C_{4f}/T and $\chi(T)$ diverges with decreasing temperature.

II. METHODS

Polycrystalline samples of $Ce(Cu_{1-x}Co_x)_2Ge_2$ for $0 \leqslant x \leqslant 1$ were prepared by arc-melting the constituent elements, taken in proper ratio, in an argon atmosphere. Some of the samples were subjected to heat treatment in evacuated sealed quartz tubes at 850 °C for one week. We found that the residual resistivity of the homogenized ingots is significantly lower than that of the as-cast specimens. The results presented here were obtained on the annealed specimens. Powder x-ray diffraction with Cu-K_α radiation was used to determine the phase purity and crystal structure. A scanning electron microscope (SEM) equipped with energy dispersive x-ray (EDX) analysis was used to check the homogeneity and composition of the samples. The magnetic measurements in the temperature range 2 K to 300 K were carried out using a commercial vibrating sample magnetometer (VSM) attached to a physical property measurement system (PPMS; Quantum Design), whereas measurements in the temperature range 0.4 K to 2 K were accomplished in a Quantum Design SQUID magnetometer equipped with a helium-3 option. The specific heat was measured with the relaxation method in PPMS. Electrical resistivity measurements in the temperature range 2 K to 300 K were performed using the standard dc transport option of the PPMS. We used 5 mA current for the resistivity measurements down to 2 K. There is no overheating effect and the resistance is independent of the excitation current up to 5 mA as evidenced by a linear current-voltage characteristic at 2.5 K. Thermoelectric power (TEP) was measured using the thermal transport option (TTO) of the PPMS using the thermal relaxation method. A heat pulse of 30 seconds was applied to raise the temperature of the hot end by 3% of the base temperature.

III. RESULTS AND DISCUSSION

Powder x-ray diffraction patterns of $Ce(Cu_{1-x}Co_x)_2Ge_2$ for $0 \leqslant x \leqslant 1$ (Fig. 1) confirm that each member of the series is single-phase crystallizing in the $ThCr_2Si_2$-type tetragonal structure with space group $I4/mmm$. The lattice parameters for $x = 0$ and $x = 1$ are in good agreement with the values reported in literature for $CeCu_2Ge_2$ [4] and $CeCo_2Ge_2$ [24], respectively. The lattice volume [Fig. 2(b)] is found to decrease continuously for the entire x without any change in crystal structure, though the c axis expands beyond $x \sim 0.5$ [Fig. 2(a)]. A clear change of slope in the x dependence of lattice volume around $x = 0.6$ is observed, signaling a change in the cerium valence. The relative change in the volume from $x = 0$ to 0.6 is about -2.5%. The volume contraction results in a chemical pressure which can be calculated using the Birch-Murnaghan equation $P = B_0 \Delta V(x)/V(0)$, where B_0 is the bulk modulus and its value for $CeCu_2Ge_2$ is reported to be 98 GPa [25]. The estimated value of chemical pressure thus comes out to be $P = 2.6$ GPa for $x = 0.6$ and $P = 4.9$ GPa at $x = 1.0$.

Magnetization $M(T)$ measurements were carried out for $Ce(Cu_{1-x}Co_x)_2Ge_2$ at a fixed applied field of $H = 0.1$ T

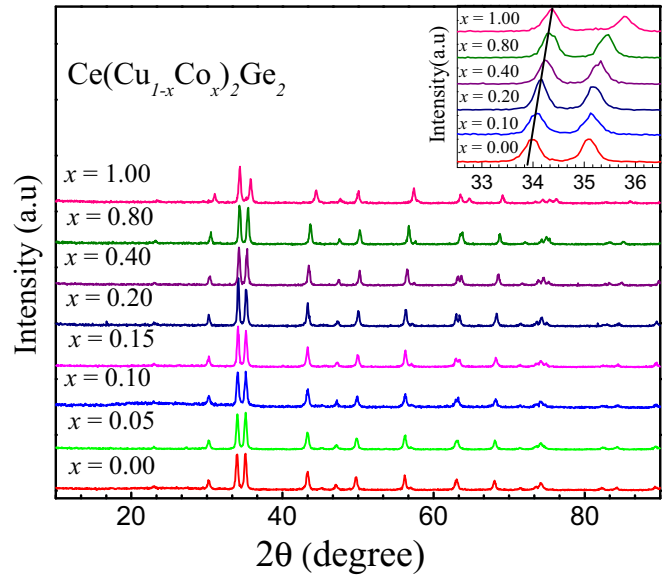

FIG. 1. Room-temperature x-ray diffraction pattern of $Ce(Cu_{1-x}Co_x)_2Ge_2$. Inset shows the shifting of peaks with Co doping.

and the resulting susceptibilities $\chi(T) = M(T)/H$ for $x = 0$, 0.02, 0.05, 0.1, 0.2, and 0.3 are plotted in Fig. 3. The upper right inset of Fig. 3 shows $\chi(T)$ of $x = 0.2$ and 0.4 down to 0.4 K whereas the lower left inset shows inverse susceptibility as a function of temperature for $x = 0.4$, 0.6, 0.8, and 1. The antiferromagnetic transition temperature, also referred to as the Néel temperature T_N, is defined by the pronounced maxima (indicated by arrows) in $\chi(T)$. T_N is found to shift towards low temperature with increasing x. For $x \geqslant 0.4$ no anomaly due to magnetic ordering is found down to 0.4 K. It

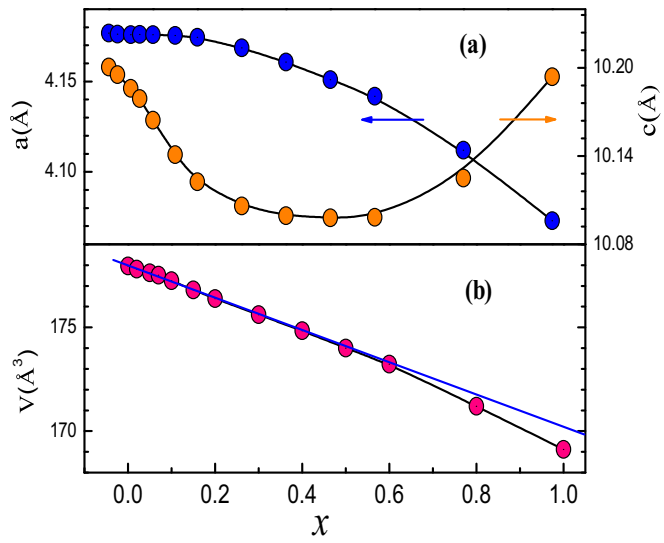

FIG. 2. Lattice parameters (upper panel) and volume (lower panel) of $Ce(Cu_{1-x}Co_x)_2Ge_2$ at room temperature as a function of Co concentration x. Solid lines passing through the symbols are a guide to the eyes. A change of slope in $V(x)$ is seen around $x = 0.6$ in the lower panel.

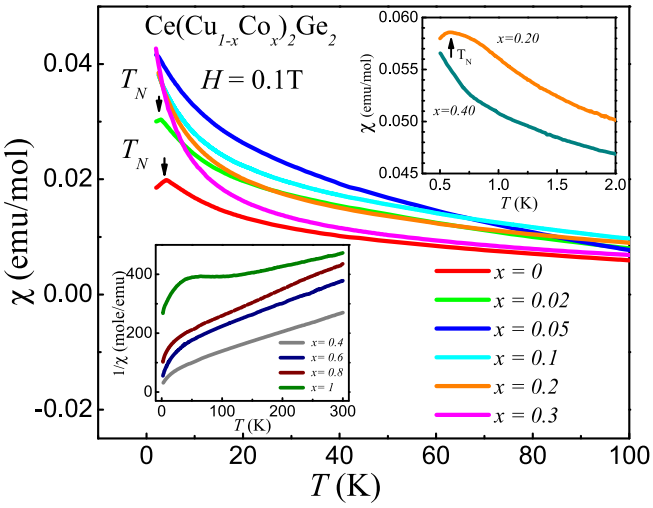

FIG. 3. Temperature dependence of the magnetic susceptibility for $x = 0$, 0.02, 0.05, 0.1, 0.2, and 0.3. The AFM transition temperatures T_N are marked by arrows. The upper right inset shows the data for $x = 0.2$ and 0.4 in the millikelvin temperature range whereas the lower left inset shows inverse susceptibility data for $x = 0.4$, 0.6, 0.8, and 1.

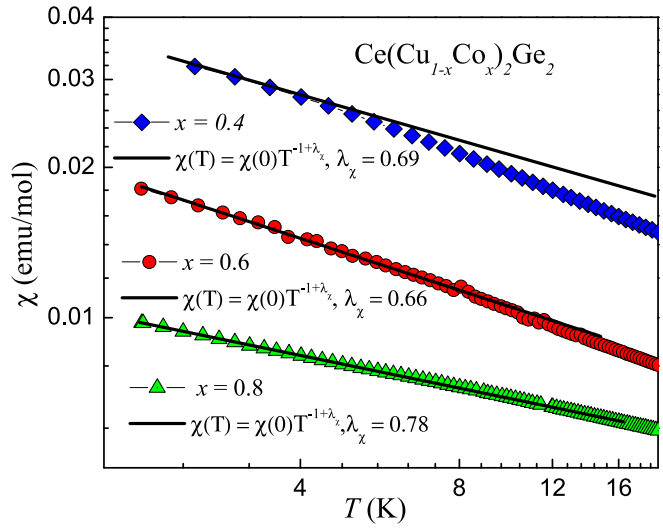

FIG. 4. Temperature dependence of the magnetic susceptibility of $Ce(Cu_{1-x}Co_x)_2Ge_2$ for $x = 0.4$, 0.6, and 0.8.

is important to note that unlike $Ce(Cu_{1-x}Ni_x)_2Ge_2$ [20,21,26] we have not observed a further increase of T_N or even two different T_N simultaneously for intermediate concentrations down to 0.4 K. At high temperature ($T > 200$ K), the susceptibility follows modified Curie-Weiss behavior [$\chi = \chi_0 + C/(T - \theta_P)$]. Here χ_0 is the temperature-independent term and $C = N\mu_{\text{eff}}^2/3k_B$, where μ_{eff} is the effective moment. The Curie-Weiss temperatures θ_P obtained from the fits of the high-temperature (200 K $\leqslant T \leqslant$ 300 K) susceptibilities with the above equation for $0 \leqslant x \leqslant 1$ are presented in Table I. With increasing Co concentration, θ_P increases to a value of -105 K at $x = 0.6$ and then to even larger negative values of -399 K for $x = 1$. This is a common feature in Ce-based materials with strong hybridization between the $4f$ and conduction electrons and indicates that the Kondo interaction strengthens with increasing x [27]. Grüner and Zawadowski [28] have shown that the absolute value of θ_P is related to the Kondo temperature as $T_K = |\theta_P|/4$. From this relation we estimated the values of T_K (for $CeCu_2Ge_2$, $T_K = 6$ K and for $CeCo_2Ge_2$, $T_K = 100$ K), which are very similar to those reported in the literature [5,23,29]. T_K for all concentrations are given in Table I. The effective moment of $CeCu_2Ge_2$ is found to be 2.50 μ_B. Furthermore, the effective moment (μ_{eff}) for $CeCo_2Ge_2$ and some intermediate concentrations are slightly higher than the theoretical value of Ce^{3+} (2.54 μ_B corresponding to the $J = 5/2$ multiplet of the free Ce^{3+} ion). Therefore, at high temperature the valence state of Ce is close to Ce^{3+} even for higher x values which is consistent with soft x-ray resonant photoemission investigations [29] and near-edge x-ray absorption studies [30] of $CeCo_2Ge_2$. Figure 4 shows the temperature dependence of the magnetic susceptibility of $Ce(Cu_{1-x}Co_x)_2Ge_2$ for $x = 0.4$, 0.6 [where the magnetic order is completely suppressed ($T_N \to 0$)], and 0.8 on a logarithmic (both axes) plot. The solid lines in Fig. 4 represent the least-squares fits of the Castro Neto model, i.e., $\chi(T) = \chi(0)T^{-1+\lambda_\chi}$, at low temperatures, where λ_χ is a parameter determined by the best fit. The values of λ_χ for different compositions x are given in Table II. It is to be noted that the NFL-like power-law dependence is seen even for the $x = 0.8$ sample. While these results are suggestive of quantum Griffiths singularities, further measurements at low temperature are required to verify our conjecture.

The temperature dependence of the heat capacity $C_P(T)$ of $Ce(Cu_{1-x}Co_x)_2Ge_2$ ($x = 0$, 0.05, 0.1, 0.15, 0.2, 0.3, 0.4,

TABLE I. Effective paramagnetic moments μ_{eff} (μ_B), antiferromagnetic ordering temperature T_N (K), Curie-Weiss temperature θ_P (K), and Kondo temperature T_K (K) obtained from susceptibility (T_K^χ), magnetoresistance scaling (T_K^{MR}), and entropy (T_K^S) of $Ce(Cu_{1-x}Co_x)_2Ge_2$.

x	μ_{eff} (μ_B)	θ_P (K)	T_N (K)	T_K^χ (K)	T_K^{MR} (K)	T_K^S (K)
0	2.50	−25.2	4.1	6.3		7
0.02	2.54	−26.2	3.0	6.5		
0.05	2.66	−30.2	2.1	7.5	6.7	6
0.1	2.59	−35.8		8.9		6
0.15	2.71	−37.7		9.4	7.8	
0.2	2.59	−35.8	0.6	8.9	8.5	8
0.4	2.8	−60.0		15.0		13
0.6	2.53	−105.4		26.4	24.7	19
0.8	2.61	−156.4		39.0	36.3	≈24
1	2.69	−399.8		99.7		>50

TABLE II. Exponent λ obtained from fits with power laws $C/T = aT^{-1+\lambda}$ to specific heat (λ_C) and magnetic susceptibility (λ_χ) data of $Ce(Cu_{1-x}Co_x)_2Ge_2$ for $x = 0.4$, 0.6, and 0.8.

x	0.4	0.6	0.8
λ_C		0.53	0.56
λ_χ	0.69	0.66	0.78

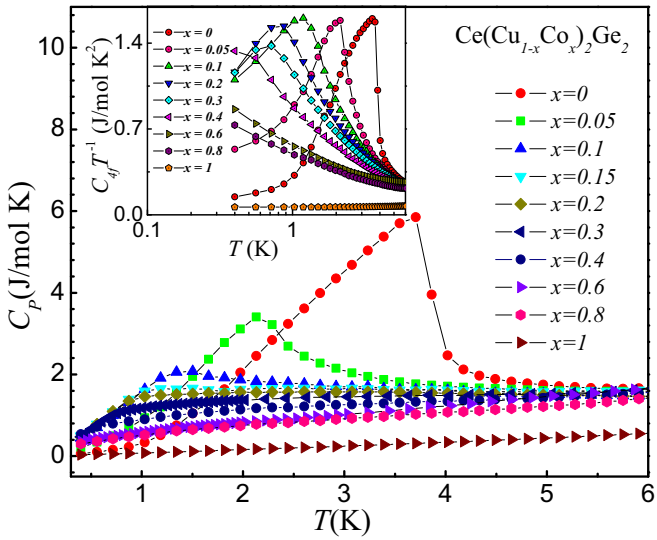

FIG. 5. Low-temperature specific heat of $Ce(Cu_{1-x}Co_x)_2Ge_2$ for $x = 0$, 0.05, 0.1, 0.15, 0.2, 0.3, 0.4, 0.6, 0.8, 1 in the temperature range of 0.4 K to 6 K. Inset shows C_{4f} divided by T vs log$T$ for $x = 0$, 0.05, 0.1, 0.2, 0.3, 0.4, 0.6, 0.8, and 1.

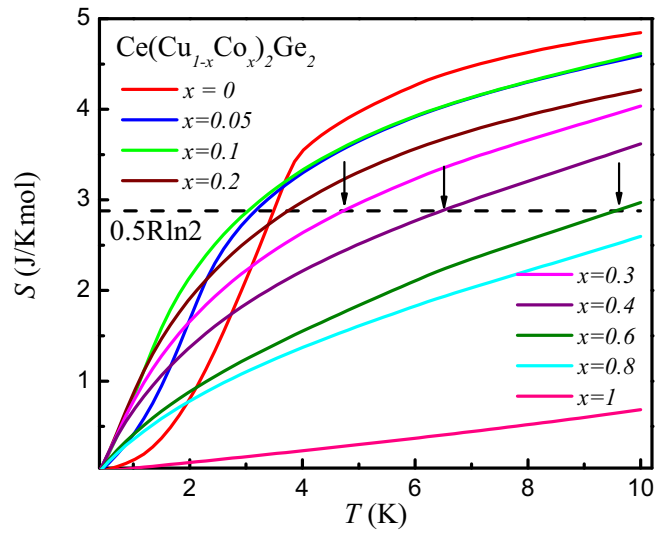

FIG. 6. The magnetic $(4f)$ entropy (S_{mag}) as a function of temperature obtained from the heat capacity data as described in the text.

0.6, 0.8, 1) down to 0.4 K is shown in Fig. 5. The magnetic part of the heat capacity $C_{4f}(T)$ was deduced by subtracting the heat capacity of $LaCu_2Ge_2$ and $LaCo_2Ge_2$ from that of $Ce(Cu_{1-x}Co_x)_2Ge_2$ after adjusting the renormalization to account for the slight atomic mass difference between La, Ce, Co, and Cu, as follows:

$$C_{\rm mag}[x] = C_P[x] - (1-x) \times C_P[{\rm LaCu_2Ge_2}] - (x) \times C_P[{\rm LaCo_2Ge_2}]. \quad (1)$$

The inset of Fig. 5 shows C_{4f}/T vs T for $x = 0$, 0.05, 0.1, 0.2, 0.3, 0.4, 0.6, 0.8, and 1. The low-temperature anomaly in $C_P(T)$ as well as in $C_{4f}(T)$ is associated with the antiferromagnetic transition T_N for $0 \leqslant x \leqslant 0.4$. For $x > 0.4$, the specific heat exhibits no anomaly down to 0.4 K. As T_N approaches zero around $x_c = 0.6$, C_{4f}/T diverges down to 0.4 K, the lowest temperature at which the data were recorded. This is a common feature of non-Fermi-liquid behavior near a QCP in correlated f-electron materials and associated with quantum critical fluctuation of the magnetic order parameter. The magnetic contribution to the entropy $S_{\rm mag}$, calculated by integrating the C_{4f}/T versus T, is shown in Fig. 6. The value of entropy for $x = 0.00$ is $0.6R\ln 2$ at $T = 4$ K and $0.8R\ln 2$ at 10 K. The reduced value of magnetic entropy suggests the presence of Kondo screening of the f moment by the conduction electrons even in the magnetically ordered state [31]. The full entropy expected for the $J = 5/2$ multiplet of Ce^{3+} is recovered at room temperature [32]. The black arrows indicate the position of the Kondo temperature $(T_K/2)$ estimated using the relation $T_K = 2T(S = 0.5R\ln 2)$ [33] and the obtained values are listed in Table I. The C_{4f}/T vs T data for $Ce(Cu_{0.4}Co_{0.6})_2Ge_2$, located at the magnetic-nonmagnetic boundary, are shown in the main panel of Fig. 7. The upper right inset of Fig. 7 shows the C_{4f}/T vs T data for $Ce(Cu_{0.2}Co_{0.8})_2Ge_2$ on a log-log plot. The data for both $x = 0.6$ and 0.8 have been fitted with a power law $C_{4f}/T = aT^{-1+\lambda_C}$ in the temperature range 0.4 K $\leqslant T \leqslant$ 4 K and the obtained values of λ_C are listed in Table II. We note that there is a discrepancy in the values of λ_C inferred from the fits to magnetization and heat capacity data. Similar discrepancies have also been observed by Castro Neto [13], which were attributed to magnetocrystalline anisotropy and the preferred crystalline orientation in polycrystalline samples. In order to provide a direct comparison between power-law and logarithmic behavior at critical concentration x_c, C_{4f}/T vs T is presented in the lower left inset of Fig. 7 on the logarithmic scale. A logarithmic divergence corresponding to 2D fluctuations has also been observed experimentally for several NFL systems in the crossover regime near an AFM QCP

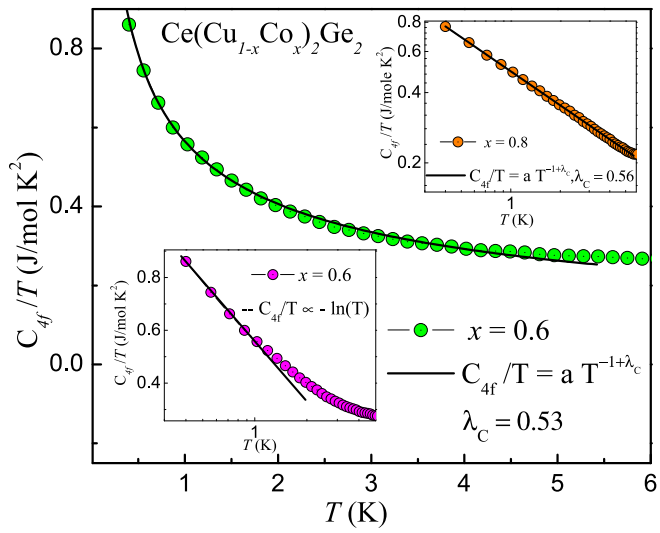

FIG. 7. Low-temperature specific heat of $CeCu_{0.8}Co_{1.2}Ge_2$. The upper right inset shows the specific heat of $CeCu_{0.2}Co_{1.6}Ge_2$ on log-log plot. The solid lines are fit to the data with $C_{4f}/T \propto T^{-1+\lambda_C}$ behavior. Lower inset shows C_{4f}/T vs the logarithm of T for $CeCu_{0.8}Co_{1.2}Ge_2$ and is fitted by $C_{4f}/T \sim -\ln(T)$ (solid line).

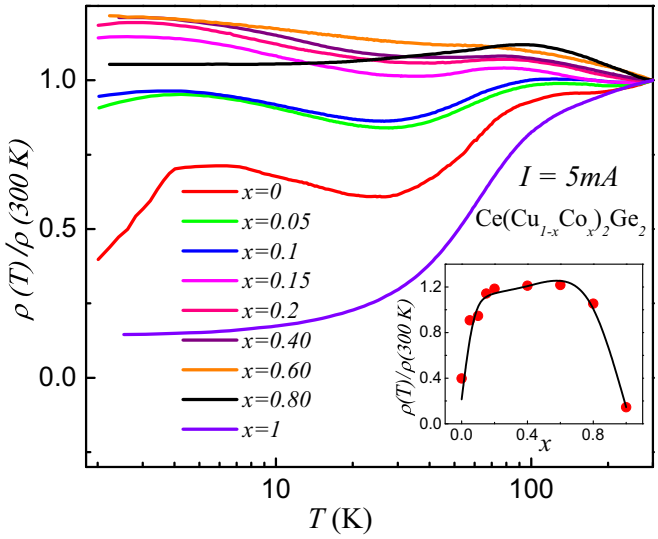

FIG. 8. Temperature dependence of the resistivity normalized to the room-temperature value for $0 \leqslant x \leqslant 1$. Inset shows $\rho(2\ \mathrm{K})/\rho(300\ \mathrm{K})$ vs x. Solid line passing through the symbols is a guide to the eyes.

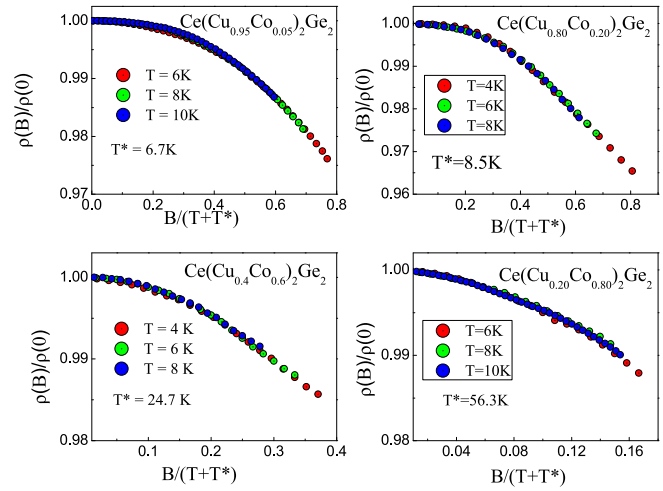

FIG. 9. Normalized resistivity plotted as a function of $\mu_0 H/(T + T^*)$ for $x = 0.05$, 0.2, 0.6, and 0.8, where T^* is the characteristic temperature.

[13,17]. From the lower inset of Fig. 7, it is clear that the data follow the function $C_{4f}/T = -a\ln(T)$ in a comparatively small temperature range 0.4 K $\leqslant T \leqslant$ 1.0 K which is not entirely convincing. Our data for $x = 0.6$ are also in marked contrast to the asymptotic ($T \to 0$) dependencies predicted by the spin-fluctuation theory at the AFM QCP in 3D [14,16], namely, $C_{4f}/T \propto 1 - a\sqrt{T}$. Thus, for concentrations near $x \sim 0.6$, an AFM QCP is observed in this series and NFL behavior becomes evident as inferred from the power-law dependence over a significant temperature range. For $CeCo_2Ge_2$ we obtain $\lambda = 1$, as expected for a Fermi liquid behavior.

Figure 8 shows the temperature dependence of the normalized electrical resistivity of $Ce(Cu_{1-x}Co_x)_2Ge_2$ in the range $0 \leqslant x \leqslant 1$. The broad but well-defined maximum at around $T_{CF} = 100$ K is due to the crystal field (CF) effect. The low-temperature maximum ($T_{\max}$) at around 6 K is attributed to Kondo coherence. It is monotonically decreasing with increasing x in sharp contrast to increase in $T_{\max}$ in $CeCu_2(Si_{1-x}Ge_x)_2$ [6] and $CeCu_2Ge_2$ under pressure [34]. For the Co-doped samples, the resistivity at 2 K is approximately the same as that around 300 K and we did not observe a large resistance drop associated with Kondo coherence at least down to 2 K. We believe that the decrease in the value of the residual resistivity ratio $[\rho(2\ \mathrm{K})/\rho(300\ \mathrm{K})]$ is due to a dominating Kondo-type scattering at low temperature as in the case of $CePd_{1-x}Rh_x$ [27] and $Ce(Pd_{1-x}Ni_x)_2P_2$ [10]. The low-temperature resistivity data of Ref. [22] confirm the deviation from FL for $x = 0.6$ whereas $Ce(Cu_{1-x}Co_x)_2Ge_2$ recovers its FL nature for $x \geqslant 0.8$ [22,23], where the resistivity follows a quadratic temperature dependence $\rho(T) - \rho(0) = \Delta\rho = AT^2$ (not shown here). The x dependence of $\rho(2\ \mathrm{K})/\rho(300\ \mathrm{K})$ is shown in the inset of Fig. 8, where $\rho(2\ \mathrm{K})/\rho(300\ \mathrm{K})$ has a maximum value for $x_c = 0.6$.

One can estimate the Kondo temperature by carefully analyzing the magnetoresistance (MR) data. It is clear from previous studies on $CeCu_2Ge_2$ [35] that the magnetoresistance is positive in the magnetically ordered state, whereas it is negative in the paramagnetic state. The positive magnetoresistance in the ordered state is consistent with the antiferromagnetic nature of the magnetic ordering. In the paramagnetic region, the negative magnetoresistance is due to the freezing out of spin-flip scattering in a Kondo compound by the magnetic field. Figure 9 represents the normalized magnetoresistance measured in the paramagnetic state plotted as a function of $\mu_0 H/(T + T^*)$ for $x = 0.05$, 0.2, 0.6, and 0.8, which allows us to map MR data measured at different temperatures (well above AFM ordering) onto a single curve. Here, T^* is the characteristic temperature which is an approximate measure of the Kondo temperature (T_K) [36]. Thus estimated values of T_K for different concentrations are in good agreement with the T_K values inferred from magnetic susceptibility and heat capacity data and they are listed in Table I.

The temperature-dependent thermopower $S(T)$ of $Ce(Cu_{1-x}Co_x)_2Ge_2$ for $x = 0$, 0.1, 0.2, 0.4, and 0.6 is shown in Fig. 10. The data for $CeCu_2Ge_2$ are in good agreement with the literature [1,37]. $S(T)$ for $x = 0$, 0.1, and 0.2 shows a broad maximum around 90 K along with a sign change at 34 K and a minimum with the negative value of the Seebeck coefficient equal to $-8\ \mu$V/K for $x = 0.00$ and $-2.5\ \mu$V/K for $x = 0.10$. The negative peak in the thermopower below 30 K is attributed to Kondo scattering on the crystal field ground state [1]. It becomes less pronounced with increasing x and for $x = 0.4$, 0.6, and 0.8 (inset of Fig. 10), we observed only the broad maxima. The thermopower is positive and significantly enhanced for $x = 1$ (inset of Fig. 10), which is found in several Ce-based intermediate valence systems like $CeNi_2Si_2$ [38,39] and $CePd_3$ [40]. A similar feature in thermopower is also seen for $CeCu_2Ge_2$ under pressure [41], where the low-temperature negative peak disappears and becomes positive in the pressure range of 7.8 GPa to 11.2 GPa. It is important to note that in the p-T phase diagram of $CeCu_2Ge_2$ the disappearance of AFM order and emergence of the superconducting phase have been found in the same pressure range [2]. Furthermore, the thermoelectric properties

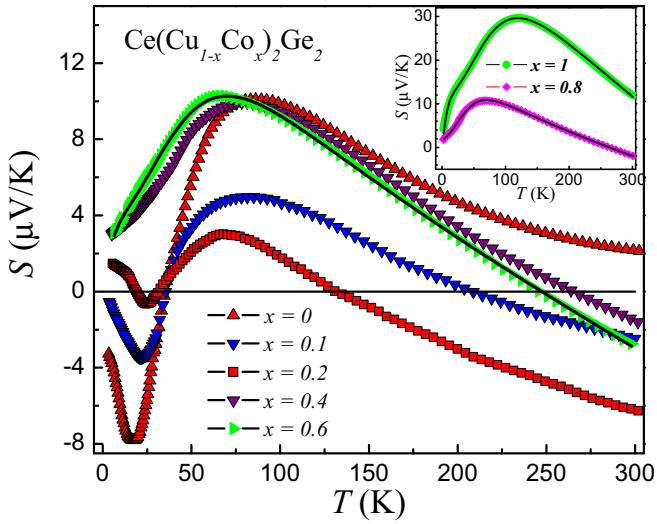

FIG. 10. Temperature dependence of thermoelectric power for $x = 0$, 0.1, 0.2, 0.4, and 0.6. The thermopower for $x = 0.8$ and 1 is shown in the inset. Solid lines are fits to the data using Eq. (3).

of many Ce- and Yb-based intermediate valence system are well described using a phenomenological valence-fluctuation model [42–44]. In this model, a Lorentzian-shaped $4f$ band is located at the energy ϵ_f ($k_B T_0$) below the Fermi level, where T_0 is the temperature-independent parameter in the intermediate valence regime. The width of the band Γ, which is proportional to the number of states that would effectively take part in the scattering process, depends on temperature as $\Gamma = T_f \exp(-T_f/T)$. Here T_f is a parameter related to the quasielastic linewidth, arising from the hybridization between the $4f$ electrons (forming a narrow band) and the surrounding conduction electrons (forming a broad band). The thermopower can be described by the function

$$S(T) = \frac{C_1 T_0 T}{T_0^2 + \Gamma(T)^2} + C_2 T, \tag{2}$$

where C_1 and C_2 are temperature-independent parameters that determine the strength of the contributions from the nonmagnetic and magnetic scattering processes, respectively. Now, $S(T)$ data for $x = 1$, 0.8, and 0.6 cannot be modeled by Eq. (2) due to the presence of an additional humplike feature below 50 K. Therefore we used an additional quasiparticle-like term [45] given by the formula $S(T) = AT/(B+T^2)$, where $A = 2\epsilon_f/|e|$ and $B = 3(\epsilon_f^2 + \Gamma^2)/(\pi^2 k_B^2)$ are the temperature-independent parameters. Therefore, the total $S(T)$ could then be expressed as

$$S(T) = \frac{C_1 T_0 T}{T_0^2 + \Gamma(T)^2} + C_2 T + \frac{AT}{B + T^2}. \tag{3}$$

Equation (3) well replicates the observed $S(T)$ data for $x = 1$, 0.8 (inset of Fig. 10), and 0.6 (Fig. 10). Indeed, the two phenomenological terms (first and last terms) in Eq. (3) are associated with two energy scales in the system. The first term is associated with a high-temperature ($T \geqslant T_K/2$) energy scale that characterizes a fully degenerate crystal field (CF) split state, whereas the last terms characterize the CF ground state at low temperature ($T \leqslant T_K/2$) [46]. The low-temperature energy scale is due to the Kondo effect, which leads to a maximum or hump in $S(T)$ at $T_K/3$ [47,48]. The low-temperature hump in $CeCo_2Ge_2$ ($T_K \sim 100$ K) at around $T = 30$ K is thus due to the Kondo effect on the CF ground state. The high-temperature maximum, due to the excited CF state, is very common in Ce-based intermediate valence systems, e.g., $CePt_{1-x}Ni_x$, $CeNi_2(Si_{1-x}Ge_x)_2$, and $CeRh_{2-x}Ni_xSi_2$ [38,49,50]. The parameters of the fits with the error bars are listed in Table III. The constants C_1 and C_2 are used as a scaling parameter for the absolute magnitude of the two contributions to the thermopower. The similar values of these parameters are observed in many Ce- and Yb-based valence fluctuating systems [43,44]. The obtained values of the parameters A and B are such that the third term in Eq. (3) does not affect the behavior of $S(T)$ at high temperature, as its contribution to $S(T)$ at high temperature is of the order of 10^{-1} μV/K, whereas it has a maximum contribution of 6.7 μV/K at 15 K. The observed behavior is consistent with other Ce-based valence fluctuating systems [42,51]. We note that the parameter T_f increases to 95 K and 103 K for $x = 0.6$ and 0.8, respectively, and afterwards to an even larger value of 164 K for $x = 1$. Thus this change indicates that the hybridization increases significantly with increasing Co concentration which is consistent with susceptibility and heat capacity measurements. These results suggest that the cerium valence evolves away from a purely trivalent state which is consistent with the deviation from Vegard's law of lattice volume and the humplike feature of inverse susceptibility for $x \geqslant 0.6$. A more detailed study using XANES measurements is needed to determine the valence evolution of Ce with doping level.

TABLE III. Parameters of fits of Eq. (3) to $S(T)$ data. Literature values of these parameters for $CeNi_2Si_2$, $CeSn_3$ and CeRhIn [42,43] are provided for comparison.

x	C_1 (μV/K)	C_2 (μV/K^2)	A (μV)	B (K^2)	T_f (K)	T_0 (K)
1	52(2)	−0.23(1)	185(3)	193(6)	164(3)	95(1)
0.8	15.7(1)	−0.115(5)	19(1)	142(3)	103(2)	47.6(4)
0.6	14.9(2)	−0.105(2)	31(1)	79(5)	95(1)	46.5(2)
$CeNi_2Si_2$	15	−0.005			300	150
$CeSn_3$	37	−0.07			300	83
CeRhIn	35	−0.070	697	851	210	61

Our results of electrical transport, magnetic susceptibility, heat capacity, and thermopower measurements lead to a consistent picture of the magnetic behavior of the polycrystalline $Ce(Cu_{1-x}Co_x)_2Ge_2$. The x-T phase diagram is presented in Fig. 11, where T_N shows two different slopes for $0 \leqslant x < 0.1$ (AF1, T_{N1}) and $0.1 \leqslant x \leqslant 0.6$ (AF2, T_{N2}). In the phase diagram, the point corresponding to C/T for $x = 0.5$ is taken from Ref. [22]. Pure $CeCu_2Ge_2$ also reveals two different magnetically ordered phases under external pressure [34]. In order to determine the effect of pressure (chemical) on $T_N(x)$ dependence, we can compare the lattice parameters of $CeCu_2Ge_2$ under chemical pressure [i.e., of $Ce(Cu_{1-x}Co_x)_2Ge_2$] with those of $CeCu_2Ge_2$ under hydrostatic pressure. We found that the volume of the $x = 0.6$ sample, where T_N goes to zero, is equal to that of $CeCu_2Ge_2$

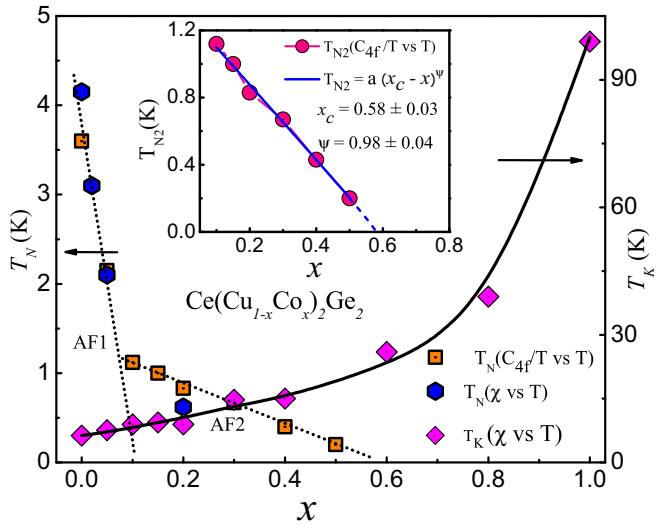

FIG. 11. Variation of AFM ordering temperature T_N (left panel) and Kondo temperature T_K (right panel) as a function of Co doping x. Inset shows T_{N2} vs x data fitted with $T_{N2} = a(x_c - x)^{\psi}$ (solid line) in the range $0.1 \leqslant x \leqslant 0.5$.

at 2.5 GPa. However, the hydrostatic pressure vs T_N phase diagram does not show any appreciable change in T_N up to the pressure of 2.5 GPa. This indicates that in $Ce(Cu_{1-x}Co_x)_2Ge_2$ the carrier concentration modification plays the major role in the suppression of magnetic ordering. The phase diagram of $Ce(Cu_{1-x}Ni_x)_2Ge_2$ [20] also shows two distinct types of antiferromagnetic ordering, representing heavy-fermion band magnetism (HFBM) and local-moment magnetism (LMM). So, in our case one can presume that the different slopes of T_N vs x in different concentration range are due to the different kinds of magnetic ordering (local and itinerant), which requires further confirmation. Furthermore, in the x-T phase diagram near a QCP the Néel temperature varies as $T_N \sim |x_c - x|^{\psi}$ with $\psi = z/(d + z - 2)$, where x is the doping concentration and z, a dynamic critical exponent relating the length and time scales of critical fluctuations [8,15,52]. The value of z is expected to be 2 and 3 for AFM and ferromagnetic (FM) QCP, respectively. The value of d equals 3 and 2 for 3D and 2D critical fluctuations, respectively. In the inset of Fig. 11, the solid line shows $T_{N2} = a(x_c - x)^{\psi}$ with $x_c \sim 0.58 \pm 0.03$ and $\psi = 0.98 \pm 0.04$ by fitting with the data of T_{N2} vs x for $Ce(Cu_{1-x}Co_x)_2Ge_2$ ($0.1 \leqslant x \leqslant 0.5$). While the linear dependence of T_N close to QCP is representative of 2D fluctuations as per HMM theory, there is no such prediction in Castro Neto's model with the disordered Griffiths phase. Our data thus call for theoretical work on the x dependence of T_N in this model. Another important observation near the QCP is the NFL behavior. In order to discuss this behavior, we have to take into account that two effects occur simultaneously in our system. One concerns the hole doping on the Cu site, which tunes the relative strengths of the Kondo and RKKY interactions, and the other manifests a disorder effect through alloying. We anticipate that the combined behavior, i.e., the competition between the Kondo effect and the RKKY interaction in the presence of disorder, could result in the formation of magnetic clusters in proximity to the QCP leading to NFL behavior which is consistent with the predictions of the model proposed by Castro Neto *et al.* The analysis of the C_{4f}/T and $\chi(T)$ suggests NFL behavior, where a power-law dependence of $C/T = aT^{-1+\lambda}$ has been found for $x = 0.6$ and 0.8. The non-Fermi-liquid effects in the specific heat and dc susceptibility are compatible with the quantum Griffiths phase scenario.

IV. CONCLUSION

We have reported a comprehensive study of electrical transport, magnetic susceptibility, heat capacity, and thermopower measurements on Co-doped $CeCu_2Ge_2$. The T_N vs x phase diagram reveals two distinct regimes that might be related to two different kinds of magnetic order. A significant deviation of physical properties from a FL behavior such as $\Delta\rho \propto T^{2\pm\delta}$ and $C/T \propto \chi(T) \propto T^{-1+\lambda}$ are observed around $x_c = 0.6$ and attributed to an AF-QCP with $T_N = 0$. We have been able to disentangle the relative importance of the influence of volume change, carrier concentration change, and disorder (Kondo disorder arising out of small variation of the Cu/Co concentration) on the physical properties. We find that the rapid decrease of T_N upon Co doping is mainly due to carrier concentration change and associated change of the T_K and T_{RKKY}. The disorder plays an important role in deciding the nature of the phase around the magnetic-nonmagnetic boundary. Instead of the standard quantum critical spin density wave found in pure heavy-fermion antiferromagnetic compounds, we found that Griffiths phase is stabilized around the critical concentration. To get more insight, experiments on single crystals are desirable. Neutron diffraction measurements are required to confirm the exact nature of magnetic ordering of the doped compounds.

ACKNOWLEDGMENTS

We gratefully acknowledge Christoph Klausnitzer for his assistance during the low-temperature magnetization measurements and D. T. Adroja, P. K. Biswas, A. D. Hiller, and J. D. Thompson for stimulating discussions.

[1] D. Jaccard, K. Behnia, and J. Sierro, Phys. Lett. A **163**, 475 (1992).
[2] D. Jaccard, H. Wilhelm, K. Alami-Yadri, and E. Vargoz, Physica B (Amsterdam) **259–261**, 1 (1999).
[3] H. Q. Yuan, F. M. Grosche, M. Deppe, C. Geibel, G. Sparn, and F. Steglich, Science **302**, 2104 (2003).
[4] F. R. de Boer, J. C. P. Klaasse, P. A. Veenhuizen, A. Bohm, C. D. Bredl, U. Gottwick, H. M. Mayer, L. Pawlak, U. Rauchschwalbe, H. Spille, and F. Steglich, J. Magn. Magn. Mater. **63–64**, 91 (1987).
[5] G. Knopp, A. Loidl, K. Knorr, L. Pawlak, M. Duczmal, R. Caspary, U. Gottwick, H. Spille, F. Steglich, and A. P. Murani, Z. Phys. B **77**, 95 (1989).
[6] G. Knebel, C. Eggert, D. Engelmann, R. Viana, A. Krimmel, M. Dressel, and A. Loidl, Phys. Rev. B **53**, 11586 (1996).

[7] Y. Ikeda, S. Araki, T. C. Kobayashi, Y. Shimizui, T. Yanagisawa, and H. Amitsuka, J. Phys. Soc. Jpn. **81**, 083701 (2012).

[8] T. Moriya and J. Kawabata, J. Phys. Soc. Jpn. **34**, 639 (1973); **35**, 669 (1973); J. A. Hertz, Phys. Rev. B **14**, 1165 (1976); A. J. Millis, *ibid.* **48**, 7183 (1993).

[9] K. Ghosh, C. Mazumdar, R. Ranganathan, and S. Mukherjee, Sci. Rep. **5**, 15801 (2015).

[10] Y. Lai, S. E. Bone, S. Minasian, M. G. Ferrier, J. Lezama-Pacheco, V. Mocko, A. S. Ditter, S. A. Kozimor, G. T. Seidler, W. L. Nelson, Y.-C. Chiu, K. Huang, W. Potter, D. Graf, T. E. Albrecht-Schmitt, and R. E. Baumbach, Phys. Rev. B **97**, 224406 (2018).

[11] V. V. Krishnamurthy, K. Nagamine, I. Watanabe, K. Nishiyama, S. Ohira, M. Ishikawa, D. H. Eom, T. Ishikawa, and T. M. Briere, Phys. Rev. Lett. **88**, 046402 (2002).

[12] M.-T. Tran and Ki-Seok Kim, J. Phys.: Condens. Matter **23**, 425602 (2011).

[13] M. C. de Andrade, R. Chau, R. P. Dickey, N. R. Dilley, E. J. Freeman, D. A. Gajewski, M. B. Maple, R. Movshovich, A. H. Castro Neto, G. Castilla, and B. A. Jones, Phys. Rev. Lett. **81**, 5620 (1998).

[14] H. v. Lohneysen, A. Rosch, M. Vojta, and P. Wolfle, Rev. Mod. Phys. **79**, 1015 (2007).

[15] A. H. Castro Neto, G. Castilla, and B. A. Jones, Phys. Rev. Lett. **81**, 3531 (1998).

[16] T. Moriya and T. Takimoto, J. Phys. Soc. Jpn. **64**, 960 (1995).

[17] K. Heuser, E. W. Scheidt, T. Schreiner, and G. R. Stewart, Phys. Rev. B **57**, R4198 (1998).

[18] E. Bauer, R. Hauser, A. Galatanu, H. Michor, G. Hilscher, J. Sereni, M. G. Berisso, P. Pedrazzini, M. Galli, F. Marabelli, and P. Bonville, Phys. Rev. B **60**, 1238 (1999).

[19] E. Svanidze, T. Besara, J. K. Wang, D. Geiger, L. Prochaska, J. M. Santiago, J. W. Lynn, S. Paschen, T. Siegrist, and E. Morosan, Phys. Rev. B **95**, 220405(R) (2017).

[20] A. Loidl, A. Krimmel, K. Knorr, G. Sparn, M. Lang, C. Geibel, S. Horn, A. Grauel, F. Steglich, B. Welslau, N. Grewe, H. Nakotte, F. R. de Boer, and A. P. Murani, Ann. Phys. **504**, 78 (1992).

[21] G. Sparn, R. Caspary, U. Gottwick, A. Grauel, U. Habel, M. Lang, M. Nowak, R. Schefzyk, W. Schiebeling, H. Spille, M. Winkelmann, A. Zuber, F. Steglich, and A. Loidl, J. Magn. Magn. Mater. **76–77**, 153 (1988).

[22] K. Maeda, H. Sugawara, T. D. Matsuda, T. Namiki, Y. Aoki, H. Sato, and K. Hisatake, Physica B (Amsterdam) **259–261**, 401 (1999).

[23] H. Fujii, E. Ueda, Y. Uwatoko, and T. Shigeoka, J. Magn. Magn. Mater. **76-77**, 179 (1988).

[24] T. Ooshima and M. Ishikawa, J. Phys. Soc. Jpn. **67**, 3251 (1998).

[25] C. Wassilew-Reul, M. Kunz, M. Hanfland, D. Hausermann, C. Geibel, and F. Steglich, Physica B (Amsterdam) **230–232**, 310 (1997).

[26] N. Buttgen, R. Bohmer, A. Krimmel, and A. Loidl, Phys. Rev. B **53**, 5557 (1996).

[27] J. G. Sereni, T. Westerkamp, R. Kuchler, N. Caroca-Canales, P. Gegenwart, and C. Geibel, Phys. Rev. B **75**, 024432 (2007).

[28] G. Gruner and A. Zawadowski, Rep. Prog. Phys. **37**, 1497 (1974).

[29] F. Venturini, J. C. Cezar, C. De Nadai, P. C. Canfield, and N. B. Brookes, J. Phys.: Condens. Matter **18**, 9221 (2006).

[30] P. H. Ansari, B. Qi, G. Liang, I. Perez, F. Lu, and M. Croft, J. Appl. Phys. **63**, 3503 (1988).

[31] V. H. Tran and Z. Bukowski, J. Phys.: Condens. Matter **26**, 255602 (2014); Y. Ikeda, H. Yoshizawa, S. Konishi, S. Araki, T. C. Kobayashi, T. Yokoo, and S. Ito, J. Phys.: Conf. Ser. **592**, 012013 (2015).

[32] R. Felten, G. Weber, and H. Rietschel, J. Magn. Magn. Mater. **63–64**, 383 (1987).

[33] C. Klingner, C. Krellner, M. Brando, C. Geibel, F. Steglich, D. V. Vyalikh, K. Kummer, S. Danzenbacher, S. L. Molodtsov, C. Laubschat, T. Kinoshita, Y. Kato, and T. Muro, Phys. Rev. B **83**, 144405 (2011).

[34] F. Honda, T. Maeta, Y. Hirose, Y. Onuki, A. Miyake, and R. Settai, J. Korean Phys. Soc. **63**, 345 (2013).

[35] B. Zeng, Q. R. Zhang, D. Rhodes, Y. Shimura, D. Watanabe, R. E. Baumbach, P. Schlottmann, T. Ebihara, and L. Balicas, Phys. Rev. B **90**, 155101 (2014).

[36] Z. Hossain, S. Hamashima, K. Umeo, T. Takabatake, C. Geibel, and F. Steglich, Phys. Rev. B **62**, 8950 (2000).

[37] H. Hodovanets, S. L. Budko, W. E. Straszheim, V. Taufour, E. D. Mun, H. Kim, R. Flint, and P. C. Canfield, Phys. Rev. Lett. **114**, 236601 (2015).

[38] E. V. Sampathkumaran, R. Vijayaraghavan, A. Adam, Y. Yamamoto, Y. Yamaguchi, and J. Sakurai, Solid State Commun. **71**, 71 (1989).

[39] E. M. Levin, R. V. Lutziv, L. D. Finkel'shtein, N. D. Samsonova, and R. I. Yasnitskil, Fiz. Tverd. Tela **23**, 2401 (1981).

[40] D. Jaccard, M. J. Besnus, and J. P. Kappler, J. Magn. Magn. Mater. **63–64**, 572 (1987).

[41] P. Link, D. Jaccard, and P. Lejay, Physica B **225**, 207 (1996).

[42] P. Wisniewski, V. I. Zaremba, A. Slebarski, and D. Kaczorowski, Intermetallics **56**, 101 (2015).

[43] C. S. Garde and J. Ray, Phys. Rev. B **51**, 2960 (1995).

[44] A. Freimuth, J. Magn. Magn. Mater. **68**, 28 (1987).

[45] U. Gottwick, K. Gloos, S. Horn, F. Steglich, and N. Grewe, J. Magn. Magn. Mater. **47–48**, 536 (1985).

[46] V. Zlatić, R. Monnier, J. K. Freericks, and K. W. Becker, Phys. Rev. B **76**, 085122 (2007); V. Zlatić, B. Horvatić, I. Milat, B. Coqblin, G. Czycholl, and C. Grenzebach, *ibid.* **68**, 104432 (2003).

[47] D. L. Cox and N. Grewe, Z. Phys. B **71**, 321 (1988).

[48] V. Zlatić, T. A. Costi, A. C. Hewson, and B. R. Coles, Phys. Rev. B **48**, 16152 (1993).

[49] J. Sakurai, A. Iwasaki, Q. Lu, D. Ho, Y. Isikawa, J. R. Fernández, and C. Gómez Sal, J. Phys. Soc. Jpn. **71**, 2829 (2002).

[50] T. Toliński, K. Synoradzki, A. Bajorek, G. Chełkowska, M. Koterlyn, G. Koterlyn, and R. Yasnitskii, Appl. Phys. A **123**, 408 (2017).

[51] T. Toliński, V. Zlatić, and A. Kowalczyk, J. Alloys Compd. **490**, 15–18 (2010).

[52] N. D. Mathur, F. M. Grosche, S. R. Julian, I. R. Walker, D. M. Freye, R. K. W. Haselwimmer, and G. G. Lonzarich, Nature (London) **394**, 39 (1998).